S-Palmitoylation determines TMEM55B-dependent positioning of lysosomes

Sönke Rudnik[1], Saskia Heybrock[1], Paul Saftig[1], Markus Damme[1,*]

[1]Institut für Biochemie, Christian-Albrechts-Universität zu Kiel, 24098 Kiel, Germany.

ORCID ID's:

Sönke Rudnik: 0000-0003-2858-0476

Saskia Heybrock: 0000-0002-5871-188X

Paul Saftig: 0000-0003-2637-7052

Markus Damme: 0000-0002-9699-9351

*Corresponding author: PD Dr. Markus Damme

Christian-Albrechts-University Kiel, Institute of Biochemistry, Olshausenstr. 40, 24098 Kiel Germany; Tel: +49 431 880 2218; mail: mdamme@biochem.uni-kiel.de

Summary statement

The lysosomal membrane TMEM55B mediates the transport of lysosomes. Here we show that TMEM55B undergoes S-palmitoylation at multiple cysteine residues, and S-palmitoylation mediates the transport of TMEM55B from the Golgi apparatus to lysosomes.

Abstract

The spatio-temporal cellular distribution of lysosomes depends on active transport mainly driven by microtubule-motors such as kinesins and dynein. Different protein complexes attach these molecular motors to their vesicular cargo: TMEM55B, as an integral lysosomal membrane protein, is a component of such a complex mediating the retrograde transport of lysosomes by establishing an interaction with the cytosolic scaffold protein JIP4 and dynein/dynactin. Here we show that TMEM55B and its paralog TMEM55A are S-palmitoylated proteins and lipidated at multiple cysteine-residues. Mutation of all cysteines in TMEM55B prevents S-palmitoylation and causes the retention of the mutated protein in the Golgi-apparatus. Consequently, non-palmitoylated TMEM55B is no longer able to modulate lysosomal positioning and the perinuclear clustering of lysosomes. Additional mutagenesis of the dileucine-based lysosomal sorting motif in non-palmitoylated TMEM55B leads to partial missorting to the plasma membrane instead of retention in the Golgi, implicating a direct effect of S-palmitoylation on the adaptor-protein-dependent sorting of TMEM55B. Our data suggest a critical role of S-palmitoylation on the trafficking of TMEM55B and TMEM55B-dependent lysosomal positioning.

Abbreviations: 2-BP, 2-bromopalmitate; 17-ODYA, 17-octadecynoic acid; Acyl-RAC, Acyl-Resin Assisted Capture; DRM, detergent-resistant membranes; LE, late endosomes; MEF, mouse embryonic fibroblast; MTOC, microtubule organizing center; PEG; polyethylene glycol; PAT, palmitoyl-acyl transferase;

Keywords: TMEM55A, TMEM55B, S-palmitoylation, lysosomal positioning, Acyl-RAC

Introduction

Lysosomes and late endosomes (LE) are highly dynamic organelles. Their spatio-temporal distribution depends on active transport mainly driven by microtubule-motors such as kinesins and dynein (Bonifacino and Neefjes, 2017; Saftig and Puertollano, 2020). Continuous transport of lysosomes within the cell is essential for the maintenance of various cellular functions such as the fusion of lysosomes with autophagosomes or with the plasma membrane (lysosomal exocytosis), respectively, the tubulation of lysosomes, and the formation of contact sites with other organelles like the endoplasmic reticulum (Ballabio and Bonifacino, 2020; Saftig and Puertollano, 2020). Various motor protein/cargo-complexes mediating the microtubule-dependent positioning of lysosomes have been described: Kinesin 1 and Kinesin 3 facilitate the anterograde transport of lysosomes. These protein complexes depend on the cytosolic BLOC-one-related complex (BORC) (Guardia et al., 2016). BORC interacts with the Ragulator complex, which is attached to the lysosomal membrane by N-myristoylation (Pu et al., 2017; Pu et al., 2015). ARL8B, a small GTPase, recruits the BORC complex and its effector SKIP/PLEKHM2, which directly interacts with Kinesin 1.

Dynein is the only retrograde microtubule motor. GTP-activated membrane-bound RAB7, which resides on the lysosomal membrane, recruits its effectors, “Rab-interacting lysosomal protein” (RILP) and PLEKHM1, to promote dynein-driven retrograde transport of LE/lysosomes. Another protein complex mediating retrograde transport of LE/lysosomes independent of RAB7 depends on the integral lysosomal membrane protein TMEM55B and the cytosolic scaffold c-Jun NH2-terminal kinase (JNK)-interacting protein 4 (JIP4, synonymously JLP). JIP4 binds to TMEM55B, thereby recruiting the dynein/dynactin complex (Willett et al., 2017). TMEM55B has two transmembrane segments, a large amino (N-) terminal cytosolic domain, a small luminal loop, and a short cytosolic carboxy (C-) terminus (**Figure 1A**). Overexpression of TMEM55B induces perinuclear clustering of lysosomes to the microtubule organizing center (MTOC), and TMEM55B knockdown leads to a more peripheral distribution of lysosomes due to increased dynein-dependent retrograde transport

processes, respectively (Willett et al., 2017). Initially, TMEM55B was assigned as a phosphatidylinositol-4,5-bisphosphate 4-phosphatase (Ungewickell et al., 2005). However, this presumed catalytic function was challenged and refuted later (Willett et al., 2017). TMEM55A is a paralog of TMEM55B, which is also localized in lysosomes. The amino acid sequences of human TMEM55A and TMEM55B are 51% identical and 63% similar. However, TMEM55A overexpression does not affect lysosomal positioning upon overexpression, implicating independent function(s) (Willett et al., 2017). Both TMEM55A and TMEM55B contain conserved dileucine-based sorting motifs close to their N-termini that mediate adaptor-protein-dependent transport. Mutagenesis of this motif leads to partial missorting of both proteins to the plasma membrane (Willett et al., 2017).

In a proteome-wide screen for TMEM55B-interacting proteins, TMEM55B was co-immunoprecipitated with subunits of the vacuolar-type proton H^+-ATPase (V-ATPase) and the Ragulator complex (Hashimoto et al., 2018), essential constituents of the mTORC1 (mechanistic target of rapamycin complex 1) signaling complex, the nutrient-sensing and signaling machinery of the cell.

TMEM55B is embedded in raft-like microdomains of membranes (Takemasu et al., 2019), a feature that is often dependent on the S-palmitoylation of transmembrane proteins (Ballabio and Bonifacino, 2020; Hashimoto et al., 2018; Takemasu et al., 2019; Zhang et al., 1998). S-palmitoylation is an important post-translational modification characterized by the reversible attachment of a C16-carbon saturated fatty acyl chain to cytoplasmic cysteine residues transferred by different palmitoyl-acyl transferases (PATs) (Charollais and Van Der Goot, 2009). Next to partitioning into membrane microdomains, S-palmitoylation often affects the intracellular trafficking and function of membrane proteins. In several proteomic studies, TMEM55A and TMEM55B were described as candidate proteins that undergo S-palmitoylation (Dowal et al., 2011; Ivaldi et al., 2012; Martin et al., 2011; Merrick et al., 2011).

Here we reveal that TMEM55A and TMEM55B are *bona fide* S-palmitoylated proteins. Under steady-state conditions, TMEM55B is present in multiple S-palmitoylated forms in different cell lines and tissues. Up to five S-palmitoylated cysteine-residues are used for the lipidation of TMEM55B. S-palmitoylation of TMEM55B is dispensable for partitioning into detergent-resistant membranes (DRM). A mutant TMEM55B protein with all cytoplasmic cysteines mutated to serine causes retention in the Golgi apparatus instead of being transported to lysosomes. Interestingly, additional mutation of the critical dileucine sorting motif of TMEM55B leads to a partial localization of TMEM55B at the plasma membrane, suggesting a critical role of S-palmitoylation in adaptor-protein-dependent post-Golgi-sorting of TMEM55B.

Results

TMEM55A and TMEM55B are both S-palmitoylated transmembrane proteins

TMEM55A and TMEM55B have been identified in proteome-wide screening studies aiming to identify S-palmitoylated proteins in different cell lines and tissues (Dowal et al., 2011; Ivaldi et al., 2012; Martin et al., 2011; Merrick et al., 2011). These findings prompted us to experimentally validate the putative S-palmitoylation of TMEM55A and TMEM55B and investigate the impact of this modification on the biology of the two proteins. To this end, we utilized a resin-assisted capture (acyl-RAC) assay that specifically enriches S-palmitoylated proteins (**Figure 1B**) (Forrester et al., 2011). In this assay, free thiols are first blocked with methyl methanethiosulfonate (MMTS), which reversibly blocks free cysteines. Thioesters are then cleaved with neutral hydroxylamine (NH_2OH), and the newly liberated thiols are captured with a thiol-reactive sepharose resin (Forrester et al., 2011). HeLa cells were transfected with hemagglutinin (HA)-tagged TMEM55B. Transfected cells were analyzed using the acyl-RAC assay followed by immunoblot of the resulting fractions (**Figure 1C**). We included control samples with cells treated with the S-palmitoylation inhibitor 2-bromopalmitate (2-BP) (Webb et al., 2000) or NaCl instead of hydroxylamine/NH_2OH in the

thioester cleavage step as negative controls. Furthermore, the presence or absence of a known S-palmitoylated protein (LAMTOR1, (Nada et al., 2009)) and a non-palmitoylated lysosomal protein (LAMP2) in these fractions was analyzed. Ectopically expressed TMEM55B-HA was robustly identified in the hydroxylamine-treated fraction containing the S-palmitoylated proteins (like LAMTOR1) but was absent in the NaCl-fraction containing non-palmitoylated proteins (like LAMP2), confirming that TMEM55B is S-palmitoylated. 2-BP treatment significantly reduced the S-palmitoylation of TMEM55B-HA, providing additional evidence for the specificity of the assay (**Figure 1C**). Like TMEM55B, TMEM55A-HA was also detected in the hydroxylamine-treated fraction, indicating that both TMEM55 paralogs undergo S-palmitoylation (**Supplemental Figure 1A**).

In an independent click-chemistry-based experimental approach, we used metabolic labeling of TMEM55B-HA expressing HeLa cells with the clickable palmitate analog 17-octadecynoic acid (17-ODYA) (Martin, 2013) (**Supplemental Figure 1B**). TMEM55B-HA was precipitated from the cell lysates via the HA-tag, and the click reaction was performed with a fluorescent dye. The samples were then analyzed by SDS-PAGE and fluorescence scanning as well as immunoblot. Metabolic labeling with varying pulse times (2 – 24 hours) revealed a band at the expected molecular weight of TMEM55B-HA (~35 kDa) with increasing pulse-time-dependent intensity. This strongly suggests the incorporation of the clickable 17-ODYA and provides direct evidence for S-palmitoylation of TMEM55B (**Supplemental Figure 1B**).

Human and mouse TMEM55B are rich in cysteines. Both contain 19 cysteine residues in total (out of 277 and 284 amino acids, respectively). These cysteine residues are unevenly distributed over the full-length protein sequence: While the very N-terminus lacks any cysteine residue, cysteines are frequent in the middle part of the protein and the first N-terminal transmembrane segment (**Figure 1A**). Notably, most cysteines are evolutionary conserved among different species, implicating essential preserved functions (**Supplemental Figure 1C**). In order to investigate whether TMEM55B is S-palmitoylated at a single cysteine residue or at multiple cysteine residues, we employed a modified acyl-RAC assay based on

the attachment of a polyethylene glycol (PEG) group on each previously S-palmitoylated cysteine after thioester cleavage (Percher et al., 2016). The attached PEG leads to a distinctive shift of the apparent molecular weight of the target protein after SDS-PAGE (Percher et al., 2016). SDS-PAGE of lysates from cells transfected with TMEM55B-HA and treated with the acyl-PEG exchange chemicals followed by immunoblot with antibodies directed against HA or TMEM55B revealed 4-6 distinct bands, each representing non-palmitoylated and differentially S-palmitoylated forms of TMEM55B with an increasing number of occupied S-palmitoylation sites as depicted in **Figure 1D**. Mono- and di-palmitoylated forms represent the most abundant species. Non-palmitoylated TMEM55B was also detectable to a substantial degree. Analysis of endogenous TMEM55B in lysates from mouse embryonic fibroblasts (MEFs) yielded similar results, excluding artifacts on S-palmitoylation due to overexpression (**Supplemental Figure 2A**). Analysis of the S-palmitoylation of different murine tissues (brain, testis, spleen) revealed a similar S-palmitoylation pattern of TMEM55B among all the tested tissues with mono- and di-palmitoylated forms as the most abundant species (**Figure 1E**). However, it should be noted that the quantification of the band intensities might be biased by the PEGylation status due to differences in the blotting procedure and might not quantitatively reflect the degree of S-palmitoylation.

Analysis of the dynamics of S-palmitoylation by a pulse-chase assay using clickable palmitate as well as parallel labeling of the protein by the clickable methionine-analog L-azidohomoalanine (AHA) revealed a similar half-life of the protein backbone and the S-palmitoylated TMEM55B (**Supplemental Figure 2B**), indicating no dynamic de- or re-palmitoylation.

Non-palmitoylated TMEM55B is retained in the Golgi apparatus rendering it unable to mediate lysosomal positioning

To more directly address the functional consequence of TMEM55B S-palmitoylation, we investigated the effect of abolishing S-palmitoylation of TMEM55B by mutating all cytosol-exposed and transmembrane embedded cysteine residues to serine (TMEM55B^{NoCys}-HA). The absence of S-palmitoylation of the TMEM55B^{NoCys}-HA construct was confirmed with the acyl-RAC assay: in contrast to wild type TMEM55B-HA, no binding of TMEM55B^{NoCys}-HA to the thiol-reactive sepharose beads was observed (**Figure 2A**). Immunoblot analysis of HeLa cells transfected with wild-type TMEM55B-HA or TMEM55B^{NoCys}-HA revealed reduced total levels of the protein lacking cysteines in the "input fractions" used for the assay (**Figure 2A**). Treating the cells with the proteasome-inhibitor MG132 rescued this effect partially and increased the levels of TMEM55B^{NoCys}-HA, indicating a fraction of non-palmitoylated TMEM55B is degraded via the proteasome (**Supplemental Figure 3A**).

We also applied the 17-ODYA labeling/click-chemistry-based approach to analyze the S-palmitoylation status of the TMEM55B^{NoCys}-HA variant (**Figure 2B**). Metabolic labeling of cells transfected with TMEM55B-HA or TMEM55B^{NoCys}-HA followed by immunoprecipitation, click-chemistry, and fluorography revealed a band at the expected molecular weight of TMEM55B-HA for the wild-type protein, but not for the TMEM55B^{NoCys}-HA, validating the absence of S-palmitoylation. In comparison to wild-type TMEM55B-HA the TMEM55B^{NoCys}-HA mutant was expressed at a lower level; however, similar levels of the tagged proteins were detected in the immunoprecipitated (IP)-fractions, indicating that the immunoprecipitation step remedied most of the difference, allowing an appropriate comparison. (**Figure 2B**). Finally, we validated the absence of S-palmitoylation of the TMEM55B^{NoCys}-HA variant in the acyl-PEG assay: In contrast to the cells transfected with wild-type TMEM55B-HA, no molecular-weight shift was observed for the TMEM55B^{NoCys}-HA in those fractions where PEG was added, and disulfide-linkages were cleaved by NH_2OH (**Supplemental Figure 3B**). As an additional control for this assay, LAMP1 and N-Ras immunoblotting were included for S-palmitoylated proteins (N-Ras) or non-palmitoylated proteins (LAMP1), respectively, additionally validating the specificity of the assay.

While the S-palmitoylation of soluble cytosolic proteins serves as a hydrophobic membrane anchor, the S-palmitoylation of membrane proteins often affects their subcellular trafficking, localization, and sorting between different organelles (Charollais and Van Der Goot, 2009; Flannery et al., 2010; Tanimura et al., 2006; Vergarajauregui and Puertollano, 2006). Therefore, we studied the trafficking of non-palmitoylated TMEM55B and analyzed if the lack of S-palmitoylation affects its subcellular localization. Under steady-state conditions, both endogenous and ectopically expressed wild-type TMEM55B is found on late endosomes and lysosomes (Willett et al., 2017), where it extensively co-localize with LAMP2 but not with other organelle maker proteins like the Golgi-marker GM130 (**Figure 2C**). Notably, TMEM55B-overexpression induces a perinuclear clustering of lysosomes due to the recruitment of the retrograde microtubule-motor complex dynein/dynactin (Willett et al., 2017). Remarkably, overexpression of TMEM55B^{NoCys}-HA shows, in contrast to the wild-type TMEM55B-HA, only little co-localization with LAMP2, but a high degree of co-localization with GM130, indicating extensive localization of non-palmitoylated TMEM55B to the Golgi apparatus (**Figure 2C**). Quantification of the images and representation of the signals as the Pearsons correlation coefficient (representing a measure of the covariance in the two signals) or the Manders overlap coefficient (as a measure of the fraction of overlapping pixels) revealed a decreased co-localization of TMEM55B^{NoCys}-HA with LAMP2 and an increased co-localization with GM130 (**Figure 2C, D**). While the transient expression of wild-type TMEM55B-HA induced robust perinuclear clustering, heterologous expression of the TMEM55B^{NoCys}-HA mutant resulted in the dispersed distribution of lysosomes throughout the cells, which was comparable to non-transfected cells (**Figure 2E**). These results indicate that (i) that lysosomal membrane localization of TMEM55B is required to exert its effect on lysosomal positioning and (ii) S-palmitoylation of TMEM55B modulates lysosomal positioning.

S-Palmitoylation is dispensable for the partitioning of TMEM55B into raft-like membrane domains

TMEM55B was previously detected in lipid rafts (Hashimoto et al., 2018). In good agreement with these findings, in MEF cells, endogenous TMEM55B exhibited a patchy and clustered distribution in the LAMP1-positive lysosomal membrane (**Figure 3A**). These findings indicate a concentration of TMEM55B in protein complexes, raft-like domains, or organelle-contact sites. In contrast, LAMP1 staining showed a rather smooth donut-like staining pattern. It should be noted that LAMTOR1, which was previously identified as a physical interactor of TMEM55B (Hashimoto et al., 2018), was found in raft-like subdomains of LEs due to its myristoylation and S-palmitoylation (Nada et al., 2009).

Palmitoylation is a major determinant of targeting proteins to raft-like subdomains of membranes (Levental et al., 2010). This prompted the question if S-palmitoylation of TMEM55B is required for its partitioning into raft-like membrane subdomains in a similar manner as for LAMTOR1. Upon sucrose-gradient fractionation of membranes from transfected HeLa cells, we confirmed the localization of TMEM55B in raft-like domains since TMEM55B-HA was enriched in fractions containing the typical detergent-resistant membrane (DRM)-marker Flotilin1 (**Figure 3B).** The non-raft protein transferrin receptor (Tfr) was absent from these DRM fractions. Endogenous TMEM55B showed an even stronger enrichment in DRMs compared to the overexpressed protein and was virtually absent from the non-raft fractions upon sucrose gradient centrifugation and analysis of the fractions by immunoblot (**Figure 3C**). Surprisingly, incubation of cells with the palmitoylation inhibitor 2-BP did not affect the partitioning of TMEM55B-HA into DRMs (**Figure 3D**), and similarly, the non-palmitoylated TMEM55B^{NoCys}-HA construct was still found in substantial amounts in the DRM fraction (**Figure 3E**). These experiments indicate that S-palmitoylation is not essential for the partitioning of TMEM55B into raft-like domains / DRMs in lysosomes.

Lack of S-palmitoylation leads to retention, but not retrieval of TMEM55B to the Golgi apparatus

Our immunofluorescence studies revealed localization of TMEM55B^{NoCys}-HA within the Golgi apparatus (**Figure 2C**), implicating either retention of the protein lacking cysteine/palmitoylation in the Golgi or rapid retrograde transport ("retrieval") from post-Golgi compartments (i.e., endosomes or LE) back to the Golgi. To investigate these two possibilities experimentally, we blocked retrograde transport through early endosomes pharmacologically by applying chloroquine. Chloroquine treatments cause swelling of endocytic compartments and interferes with retrograde transport to the Golgi, e.g. of Golgi-resident proteins like TGN46 (Chapman and Munro, 1994; Kent et al., 2012; Reaves and Banting, 1994; Reaves et al., 1998; Rous et al., 2002) (**Figure 4**). Treatment of the cells transfected with wild-type TMEM55B-HA (**Figure 4**, **upper panels**) with chloroquine resulted in perinuclear clustering of enlarged lysosomes and extensive co-localization of TMEM55B-HA and LAMP2, but no co-localization of TMEM55B-HA with GM130 or TGN46. Endogenous TGN46 displayed, in contrast to untreated cells where it co-localized with GM130, vesicular staining in the chloroquine treated cells. In contrast to TMEM5B-HA, cells transfected with TMEM55B^{NoCys}-HA showed little co-localization between HA and LAMP2 (**Figure 4, lower panels**) but extensive co-localization with GM130. Little co-localization between TMEM55B^{NoCys}-HA with TGN46 was observed in the chloroquine-treated cells. Also, strongly reduced co-localization of TGN46 and GM130 was observed, validating retention of TGN46 in post-Golgi vesicles upon chloroquine treatment. These experiments suggest that TMEM55B is retained in the Golgi apparatus rather than being transported back from post-Golgi compartments to the Golgi by retrograde transport mechanisms.

A TMEM55B mutant lacking the cytosolic domain is retained in the Golgi apparatus

Having established that TMEM55B is modified at multiple cysteine residues, we wondered which of the cysteine residues are modified by the addition of palmitate. As described above, up to five cytosolic TMEM55B cysteines are palmitoylated under steady-state conditions (**Figure 1D**). The high number of cysteines (19 in total) contained in the palmitoylation-accessible regions of the protein complicated the identification of individual palmitoylated residues. In a first attempt to address this issue, we generated constructs where all cysteine residues in the cytosolic N-terminus were mutated to serine residues (TMEM55B$^{N\text{-}term_NoCys}$-HA). Another construct was generated for the C-terminus containing the two transmembrane segments, the luminal loop and the cytosolic C-terminal tail (TMEM55B$^{C\text{-}term_NoCys}$-HA) (**Figure 5A**). Analysis of lysates from cells transfected with these constructs by immunoblot (**Figure 5B, left panel**) revealed that all constructs were expressed, though TMEM55B^{NoCys}-HA was again expressed to a significantly lower level, indicating again that cysteines are critical for stability (see also **Supplemental Figure 3)**.

Interestingly, we observed an altered migration behavior during SDS-PAGE with a minor shift towards a slightly lower apparent molecular weight for the TMEM55B$^{N\text{-}term_NoCys}$-HA variant compared with TMEM55B-HA that might be caused by altered migration behavior due to S-palmitoylation during SDS-PAGE, as observed previously for other S-palmitoylated proteins (Diez-Ardanuy et al., 2017). Analysis of lysates from cells transfected with these constructs with the acyl-RAC assay revealed specific binding of all variants to the thiol-reactive resin, qualitatively indicating S-palmitoylation of all constructs except TMEM55B^{NoCys}-HA. (**Figure 5B, right panel**). However, the TMEM55B$^{N\text{-}term_NoCys}$-HA construct is bound with lower efficiency, which might be a hint that this variant is S-palmitoylated to a lower extent as compared to the TMEM55B$^{C\text{-}term_NoCys}$-HA.

The cytosolic N-terminal domain of TMEM55B determines Golgi-export

We next analyzed the cellular localization of the TMEM55B constructs with mutations in the N- or C-terminus by immunofluorescence. In contrast to the perinuclear clustering of lysosomes induced by overexpression of wild-type TMEM55B and co-localization with LAMP2, a lack of co-localization with LAMP2 wasobserved for TMEM55B^{NoCys}-HA as described before. (**Figure 5C**). Interestingly also no co-localization between LAMP2 and the TMEM55B construct lacking cysteines in the N-terminus (TMEM55B$^{N\text{-}term_NoCys}$-HA) was observed, similar to the construct lacking all cysteines. TMEM55B$^{N\text{-}term_NoCys}$-HA showed extensive co-localization with the Golgi marker GM130 and did not alter the distribution of lysosomes (**Figure 5C**). In contrast, the construct lacking cysteines in the transmembrane domains and the C-terminus (TMEM55B$^{N\text{-}term_NoCys}$-HA) showed extensive co-localization with LAMP2 comparable to the wild-type protein and induced the typical perinuclear accumulation of lysosomes. No co-localization with GM130 was observed (**Figure 5C**).

Our data indicate that S-palmitoylation of the cytosolic N-terminal domain of TMEM55B (but not the cysteines within the transmembrane domains or cytosolic C-terminus) is critical for Golgi-export and sorting to lysosomes and indirectly critical for inducing perinuclear clustering of lysosomes.

S-Palmitoylation of TMEM55B affects adaptor protein-dependent post-Golgi sorting

The Golgi-localization of the TMEM55B^{NoCys}-HA mutant (**Figure 2C**) suggests a direct impact of S-palmitoylation on intracellular trafficking and post-Golgi sorting. As described above, the sorting of TMEM55B depends on a dileucine-based motif (ERSPLL, the critical glutamic acid, and the leucine residues L11 and L12 are underlined) within the N-terminus of TMEM55B (Willett et al., 2017) (**Figure 6A**). Dileucine-based motifs are recognized by adaptor protein complexes, facilitating the concentration of cargo into clathrin-coated vesicles and subsequent intracellular sorting. They are typically found close to transmembrane segments

of the cargo protein (Bonifacino and Traub, 2003). In TMEM55B, however, the dileucine-based motif is distal of the transmembrane domains, close to the N-terminus with a distance of more than 200 amino acids between the sorting motif and the first transmembrane domain (**Figure 6A**).

Interestingly, S-palmitoylation affects adaptor protein-dependent sorting of mucolipin-1, an ion channel and lysosomal membrane protein (Vergarajauregui and Puertollano, 2006). Palmitoylation mediates endocytosis from the plasma membrane by bringing the C-terminal endocytosis motif closer to the membrane, thus facilitating its interaction with the adaptor protein AP-2 (Vergarajauregui and Puertollano, 2006). To investigate whether S-palmitoylation of TMEM55B is required for its interaction with adaptor proteins, we analyzed the sorting of the TMEM55B^{NoCys}-HA mutant by additionally mutating the dileucine motif. The resulting TMEM55B$^{NoCys_LL/AA}$ mutant was transfected into HeLa cells, and its localization was analyzed by confocal microscopy (**Figure 6B**). In agreement with previously published results (Willett et al., 2017), TMEM55B$^{LL/AA}$ was missorted to the plasma membrane with only a minor fraction co-localizing with the lysosomal marker LAMP2 and very little co-localization with the early endosomal marker EEA1 (**Supplemental Figure 4**). TMEM55B^{NoCys} was again exclusively detected in the Golgi-apparatus (GM130 co-staining). TMEM55B$^{NoCys\ LL/AA}$ lost this exclusive Golgi localization but was instead found to a significant degree at the plasma membrane. These findings suggest that upon mutagenesis of the sorting motif and in the absence of S-palmitoylation, a sub-fraction of TMEM55B can exit the Golgi and is missorted to the plasma membrane.These experiments agree with the assumption that S-palmitoylation affects the adaptor-protein- and dileucine-dependent cellular sorting of TMEM55B.

Our experiments suggest that S-palmitoylation of the N-terminus allows the dileucine-based motif to get in closer proximity to the membrane. To support this hypothesis experimentally, we generated a construct in which the great majority of the cytosolic N-terminal domain of TMEM55B was deleted so that the dileucine-motif is forced into close proximity to the membrane (TMEM55B$^{C\text{-}term+LL}$-HA) (**Figure 6C**). In agreement with our hypothesis and in contrast to the observation that transfected TMEM55B$^{C\text{-}term}$-HA, and TMEM55B$^{C\text{-}term+LL}$-HA

are found in post-Golgi compartments, containing the lysosomal marker LAMP2 and at the plasma membrane as determined by immunofluorescence, indicating partial transport to lysosomes (**Figure 6D**). Notably, the expression of the TMEM55B$^{C\text{-}term+LL}$-HA construct did not result in lysosomal clustering. This suggests that other regions of the N-terminal domain are necessary for this “lysosomal-positioning” function

Discussion

Lysosomes are highly dynamic organelles, and their microtubule-dependent spatial distribution in the cell is orchestrated by a sophisticated system of motor proteins that need to be tightly controlled (Ballabio and Bonifacino, 2020; Bonifacino and Neefjes, 2017). The transport of these organelles is regulated by motor protein attachment and protein complexes facilitating cargo engagement (Saftig and Puertollano, 2020). Our understanding of protein complexes mediating this sophisticated system has significantly improved in the past few years, and the complex of TMEM55B and JIP4 is among the most recently characterized motor/cargo-adaptor machineries (Willett et al., 2017). How this complex is regulated, e.g., by post-translational modifications, remains to be determined. As we could demonstrate in this study, TMEM55B is subject to S-palmitoylation, a reversible post-translational modification. TMEM55B can also be modified by phosphorylation: A reversible phosphorylation by Erk/MAPK at two distinct serine residues of TMEM55B may regulate TMEM55B-dependent lysosomal positioning (Takemasu et al., 2019). The precise mechanism of how phosphorylation alters this function, however, remains enigmatic. It will be interesting to analyze in future experiments if phosphorylation and S-palmitoylation of TMEM55B reciprocally affect each other.

Though we cannot exclude a regulatory function of S-palmitoylation in general or of specific S-palmitoylation sites in regards to lysosome positioning, e.g., by modulating the interaction of TMEM55B and JIP4, we propose that S-acylation regulates the post-Golgi trafficking of TMEM55B. The closely related protein TMEM55A does not interact with JIP4 (Willett et al.,

2017), and it does not mediate lysosomal positioning. However, TMEM55A is also S-palmitoylated, indicating that S-palmitoylation is required for shared functions of the two TMEM55 proteins. Moreover, it is evident from our experiments that the block of S-palmitoylation of TMEM55B leads to complete retention of the protein in the Golgi and abrogates sorting of TMEM55B to lysosomes.

S-Palmitoylation of transmembrane proteins is well known to affect intracellular sorting and particularly facilitates post-Golgi sorting events (Ernst et al., 2019; Guardia et al., 2016). Mutation of the S-palmitoylation sites or pharmacological inhibition of S-palmitoylation of synaptotagmin VII by 2-BP blocked its trafficking to lysosomes (Flannery et al., 2010). As a proposed mechanism, an S-palmitoylation-dependent interaction with the tetraspanin CD63 was suggested, which is essential for lysosomal sorting and contains a critical lysosomal sorting motif (Flannery et al., 2010). TMEM55B might similarly require an interaction partner for post-Golgi-trafficking, and this interaction might be regulated by S-palmitoylation.

Mutagenesis of the dileucine-based sorting motif in TMEM55B leads to missorting of the protein to the plasma membrane, implicating that the dileucine motif is critical for the adaptor protein-mediated intracellular sorting to lysosomes (Willett et al., 2017). Many lysosomal integral transmembrane proteins harbor the dileucine motif in the membrane-proximal cytosolic part of the protein (Bonifacino and Traub, 2003). It is interesting that the sorting motif in TMEM55B is located distal to the transmembrane segment. This supports the idea that S-palmitoylation brings the dileucine-motif in close proximity to the membrane bilayer where it can bind to adaptor proteins (**Figure 6E)**, which also bind phosphatidylinositol membrane lipids and the membrane-bound ARF1 (Bonifacino and Traub, 2003; Ren et al., 2013).

The results of our experiments with a TMEM55B variant that only contains the C-terminus and the two transmembrane domains with the dileucine-motif in direct proximity to the membrane support this assumption. However, the lack of specific adaptor protein-mediated sorting in the Golgi (e.g., by deleting/mutating sorting motifs) typically leads to missorting of the cargo to the plasma membrane (Ballabio and Bonifacino, 2020), as observed for the

analyzed dileucine-mutated TMEM55B. Instead, retention in the Golgi was demonstrated for the palmitoylation-deficient TMEM55B mutant, arguing against this explanation. To our surprise, mutagenesis of the dileucine-motif in the non-palmitoylated TMEM55B leads to partial missorting to the plasma membrane, suggesting that S-palmitoylation plays a role in the adaptor protein-mediated sorting but that additional factors are involved. These factors might involve protein-protein interactions in the Golgi that depend on S-palmitoylation and might act independently or in concert with the adaptor-protein mediated sorting machinery. S-Palmitoylation of the integral lysosomal membrane protein mucolipin 1 mediates its adaptor protein-dependent transport by facilitating binding of the canonical motif to the membrane-proximal AP complex (Vergarajauregui and Puertollano, 2006). However, more direct effects of S-palmitoylation on protein sorting are known: Lack of S-palmitoylation of “linker for activation of T cells” (LAT), an adaptor molecule mediating T cell receptor signaling, that is palmitoylated on one or two juxtamembraneous cysteines, leads to it's retention in the Golgi (Tanimura et al., 2006). A lack of S-palmitoylation abrogates partitioning into lipid rafts (Tanimura et al., 2006), and the mutant protein was unable to traffic to the plasma membrane despite the presence of the transmembrane portion (Zhang et al., 1998), similar to TMEM55B. For non-palmitoylated TMEM55B, however, we did not observe significant alterations of its partitioning into raft-like domains, suggesting a different mechanism. In this regard, it is interesting to note that the transfected TMEM55B construct lacking cysteines in the N-terminal domain was still S-palmitoylated. A contribution of the membrane-proximal / membrane-embedded cysteine residues cannot be ruled out.

Another possibility of how S-palmitoylation might regulate post-Golgi-sorting was proposed recently: Palmitoylation of juxtamembraneous cysteines affects the membrane tilting and sorts palmitoylated proteins in unique subdomains, from which they are sorted in cargo vesicles for anterograde transport (Ernst et al., 2018). The observation that the mutant protein lacking cysteines in the C-terminus, including the two transmembrane domains, was still retained in the Golgi apparatus suggests that such a mechanism contributes to the observed trafficking defects.

The Golgi apparatus is a central hub for S-palmitoylation. Notably, 17 out of 23 DHHC PATs exhibit significant overlap with endogenous Golgi markers, and nine localized to the Golgi exclusively (Ernst et al., 2019). Future experiments will address the identification of the responsible PAT(s) for TMEM55A and TMEM55B.

Our study highlights the importance of S-acylation as a critical determinant in regulating the subcellular trafficking of lysosomal transmembrane proteins. Moreover, our findings increase our knowledge of TMEM55B and its role as a central component of the TMEM55B / JIP4-dependent retrograde sorting machinery.

Material & Methods

Reagents, plasmids, and antibodies

Antibodies: Analytical grade chemicals were purchased, if not stated otherwise, from Sigma-Aldrich (MO., USA). The following antibodies were used in the study: TMEM55B (Proteintech), HA (Roche / Sigma Aldrich), LAMP2 (clone Abl93; Developmental Studies Hybridoma Bank), GAPDH (Santa Cruz Biotechnology), N-Ras (Santa Cruz Biotechnology), Flotillin1 (BD Bioscience), TFR (Abcam), NPC1 (Abcam), GM130 (BD), Lamtor1 (Cell Signaling), EEA1 (Cell Signaling), TGN46 (Proteintech). Fluorophore-conjugated secondary antibodies against the corresponding primary antibody species (AlexaFluor 6488, AlexaFluor 594, AlexaFluor 647) were purchased from Invitrogen / Molecular Probes and were diluted 1:500. 2-Bromopalmitate and Chloroquinewere purchased from Sigma-Aldrich. cDNA coding for mouse TMEM55B or TMEM55A were cloned into the pcDNA3.1 Hygro(+).

Site-directed mutagenesis

Site-directed mutagenesis was performed according to standard protocols. A PCR mixture was prepared as followed: 1x Phusion GC buffer containing 1.5 mM $MgCl_2$ (Thermo Fisher Scientific), dNTP-mix to a final concentration of 0.2 mM, 3% DMSO (Thermo Fisher

Scientific). Overlapping forward and reverse primers (Sigma-Aldrich) containing the desired mutation were added to a final concentration of 0.2 µM, and finally, Phusion High-Fidelity DNA Polymerase (Thermo Fisher Scientific) was added. The PCR reaction was performed in a FexCycler2 PCR machine (Analytik Jena) with an annealing temperature of 54°C and an elongation temperature of 72°C. The PCR product was treated with 10 units DpnI (Thermo Scientific) for 1 h at 37°C to digest the template plasmid (methylated strand) before the transformation.

Sucrose gradient for detergent-resistant membrane-enrichment

For isolation of detergents resistant membranes, cells were harvested in PBS cOmplete™ (Roche / Signa-Aldrich) and lysed for 1 hour at 4 °C in Solution A (50 mM Tris/HCl, pH=7,4, 150 mM NaCL, 1 mM EDTA, 1 mM Natriumorthovanadate, 1 mM NaF, 0.25% (w/v) Triton X-100). The lysates were adjusted with 63.75% (w/v) sucrose in Solution A to a final concentration of 42.5% (w/v) sucrose. Sucrose in the following concentration and volumes were added on top of the lysate 1.5 mL 42.5% (w/v) sucrose; 7 mL 35% (w/v) sucrose; 2 mL 5% (w/v) sucrose. The DRMs were separated for 16 h at 4°C and 38.000 rpm in an SW41 Ti Rotor (Beckman Coulter).1 mL fractions were collected after centrifugation and prepared for further analysis.

SDS-PAGE and immunoblot

Cell lysates were prepared as described previously (Kissing et al., 2015). Proteins were separated on 10-12.5% SDS-PAGE gels and transferred to nitrocellulose membranes (Whatman, GE Healthcare, 10426994) by semi-dry blotting. The Amersham ECL Advanced Western Blotting Detection kit (GE Healthcare, RPN2135) was used for the detection of the antibody complexes.

Cell culture and transfection

HeLa cells were purchased from CLS Cell Lines Service and used at low passage numbers. HeLa and murine embryonic fibroblast (MEF) cells were cultured in Dulbecco's modified Eagle's medium (DMEM, GIBCO) supplemented with 10% (v/v) fetal bovine serum (FBS, Sigma-Aldrich) and antibiotics (Penicillin-Streptomycin) at 37°C in a humidified atmosphere at 5% CO_2. Cells were transfected with plasmid DNA with the stable cationic polymer polyethylenimine (PEI). DNA was incubated with PEI in a ratio of 1:2,5 for 20 minutes at room temperature. The solution was dripped on the adherent cells in DMEM / 10% FCS. The medium was changed 4 hours after the addition of the PEI / plasmid complex.

Acyl resin-assisted capture assay

The acyl resin-assisted capture assay (Acyl-RAC) was performed as described previously (Forrester et al., 2011) with minor modifications. Cells were harvested in PBS (contained cOmplete™ (Roche / Sigma-Aldrich) protease inhibitors) and lysed in Blocking Buffer (100 mM HEPES, 1.0 mM EDTA, 2.5% SDS, pH=7.5) by sonification two times for every 30 seconds. Free thiol-groups were blocked for 4 hours at 40°C by adding methyl-methanthiosulfonate (MMTS) with a final concentration of 0.1%. Afterward, proteins were precipitated by adding the three times volume of ice-cold acetone and incubation at -20 °C for 20 minutes followed by centrifugation 16.000x g for 2 minutes. The pellets were washed 5 times with ice-cold 70% acetone and air-dried. Protein-pellets were dissolved in 300 µL binding buffer (100 mM HEPES, 1.0 mM EDTA, 1% SDS, pH 7.5) for up to 1 hour at 40°C. Undissolved particles were pelleted for 1 minute at 16.000 xg. 30 µL of the solution was directly prepared as Input control for SDS-PAGE. 120 µL of the solution were incubated with 19 µL 2 M NaCl as a control or with 19 µL 2 M NH_2OH, pH 7.0 for cleaving palmitate-residues to generate new free thiol-groups. Proteins containing free thiol-groups were captured for 3 hours at RT by addition of Thiol Sepharose® 4B Bead-slurry in binding buffer (55mg beads + 275 µL binding-buffer = 550 µL bead-Slurry) and precipitated by

centrifugation. The pellets were washed 5 times each in 1 mL binding buffer followed by analysis by SDS-PAGE.

Acyl-polyethylene glycol exchange assay

The acyl-polyethylene glycol exchange (Acyl-PEG) assay was performed as described previously (Percher et al., 2016). Cells were harvested in PBS containing cOmplete™ protease inhibitor cocktail and lysed for 10 minutes at 37°C in 125 µL Buffer A (4% (w/v) SDS 5 mM EDTA in PBS cOmplete™) followed by addition of 375 µL Buffer B (5 mM EDTA in PBS cOmplete™). The solution was sonicated 3 times each for 20 seconds. The protein concentration was adjusted to 0.5 µg/µL by the addition of Buffer D (1% (w/v) SDS in PBS containing cOmplete™). Parts of this lysate were prepared for SDS-PAGE as input control. To reduce possible disulfide bonds, 2x 500 µL lysates were incubated for 30 minutes at RT with a final concentration of 10 mM Tris-(2-carboxyethyl)-phosphin (TCEP). Free thiol-groups were blocked for 3 hours at RT by the addition of N-Ethylmaleinimid (NEM) with a final concentration of 40 nM. Proteins were precipitated by acetone. The pellets were dissolved in 125 µL Buffer A and either incubated for 1 hour at 37°C with Buffer T (1.33 M Tris-HCl pH=7.0; 5 mM EDTA, 13 mM TCEP) as a control or with Buffer H (1.33 M Hydroxylamine pH=7.0; 5 mM EDTA, 13 mM TCEP) for cleavage of S-palmitoylation. The Proteins were precipitated by acetone. The pellets were dissolved for 1 hour at 37°C in 110 µL Buffer C (2% (w/v) SDS in PBS cOmplete™). The concentration was adjusted to 0.5 µg/µL by adding Buffer C, and the lysate was split into two 100 µL fractions. Either 10 µL of 200 mM NEM was added as control, or 10 µL of 200 mM mPEG was added to bind to the free thiol groups. Samples were incubated for 1 hour at RT. The proteins were precipitated by acetone. The pellets were solved in 1xLaemmli buffer, heat-denatured for 2 min at 95°C and used for SDS-PAGE.

Click chemistry

Click chemistry was performed as described previously (Martin, 2013). Cells were treated with 50 µM 17-ODYA in DMEM / 10% FCS for different time periods to label palmitoylated proteins, followed by immunoprecipitation of the protein of interest. For pulse-chase-labeling of palmitic acid and methionine cells were starved for 1 hour in starvation-medium (DMEM high glucose, 200µM L-cysteine, 4 mM glutamine, 1mM sodium pyruvate, 5X dialyzed FCS) followed by 2 hours of pulse in starvation-medium containing 50 µM 17-ODYA and 50 µM L-Azidohomoalanine (AHA). The chase was performed for different time periods in DMEM / 10% FCS / 2mM L-methionine / 500 µM palmitic acid, followed by immunoprecipitation of the TMEM55B-HA with an antibody against HA. Cells were lysed in IP buffer (0.1 M Phosphate buffer, pH=7.4, 1% Triton X-100 (v/v), cOmplete™) followed by sonification and precipitation of cell debris. The lysates were incubated with the primary antibodies at 4°C overnight. Magnetic protein-G coupled Dynabeads were washed 3 times with IP buffer followed by blocking overnight at 4°C in IP buffer + 5% BSA. The magnetic beads were washed 3 times with IP buffer and solved in a suitable volume of IP buffer. Lysates/AB mix was combined with the bead-slurry and incubated for 1 hour at RT. The beads were washed 3 times each 10 minutes at RT in IP buffer followed by 3 washing steps each 5 min in Reaction buffer (0.1 M Phosphate buffer, pH = 7.0). The Click-Reaction of 17-ODYA (Alkyne) with Cy3-Azide or AF647-Azide and of AHA (Azide) with AF488-Alkyne was performed according to the manual of the “CuAAC Biomolecule Reaction Buffer Kit (THPTA based)” from Jena Bioscience. In the case of double labeling, click reactions were performed sequentially.

Enrichment of membranes

A membrane preparation was performed by homogenization of cell pellets via sonification in homogenization buffer (10mM Tris pH 7.5; 140mM NaCl; 250mM Sucrose; Complete™ in H_2O). Parts of the lysate were directly adjusted to a final concentration of 1% Triton X-100 (v/v) and prepared for SDS-PAGE. The rest was separated into a soluble fraction and a membrane fraction by 100.000 xg centrifugation for 1 hour. As a washing step, the

membrane fraction was dissolved in 400 µL homogenization buffer and centrifuged at 100.000 xg for 1 hour. The pellet was solved in homogenization buffer containing 1% Triton X-100 (v/v) and prepared for SDS-PAGE.

Indirect immunofluorescence

Indirect immunofluorescence was performed as described previously (Gonzalez et al., 2018). Semiconfluent cells were grown on coverslips and fixed with 4% (w/v) paraformaldehyde (PFA; Roth) in phosphate-buffered saline PBS for 20 minutes at room temperature. After permeabilization of the cells with 0.2% (w/v) Saponin (Roth) in PBS and quenching of PFA-induced fluorescence by adding 0.12% (w/v) Glycine (Roth) in 0.2% Saponin/PBS, cells were blocked for one h with 10% fetal calf serum in 0.2 % Saponin/PBS. Coverslips were incubated overnight at 4°C with the indicated primary antibodies diluted in 0.2% Saponin/PBS. The fluorophore-coupled secondary antibodies (Alexa-Fluor-488/594/647, Thermo Fisher Scientific) were added for one hour at room temperature, followed by the embedding of the coverslips in 17% (w/v) Mowiol 4-88 Mounting Solution (Calbiochem) containing 20 mg/ml DABCO (1,4-Diazabicyclo-[2.2.2]-octane; Sigma-Aldrich) and 5µg/ml 4′,6-Diamidin-2-phenylindol (DAPI) (Sigma-Aldrich) for nuclear staining. Images were analyzed with a Zeiss Axio Observer.Z1/7 Airyscan Microscope equipped with a 40x lens (C-Apochromat 40x/1.20 W Korr). Image acquisition and processing were performed with the Zen 3.1 (blue edition) software (Carl Zeiss Microscopy GmbH, Germany).

Image quantification

The co-localization of proteins in immune fluorescence images was quantified by measuring the Pearson correlation coefficient or Manders coefficient. Single cells were framed and analyzed using Zen 3.1 (blue edition) software “Co-localization” module (Carl Zeiss Microscopy GmbH, Germany). The corresponding thresholds were optained bei single antigene stainings.

Quantitative analysis of lysosomal positioning

The distribution of LAMP2-positive organelles was measured using ImageJ Software. Cells were framed, and LAMP2-signals were measured three times in each cell by “plot profile” from the MTOC to the plasma membrane.

Statistical analyses.

If not stated otherwise, a two-tailed unpaired t-test was performed using GraphPad Prism Software Version 5.03. Significant values were considered at $P < 0.05$. Values are expressed as mean ± standard error of the mean (SEM) and significance is designated as *, $P < 0.05$; **, $P < 0.01$; ***, $P < 0.001$.

Acknowledgment

We thank Sebastian Held, Sophie Reiher, and Annika Detje for their excellent technical assistance. Laurence Abrami and Gisou van der Goot are acknowledged for discussion and help in establishing the palmitoylation assays.

Competing Interests

The authors declare no financial and non-financial competing interests.

Funding

This work was supported by the German Research Foundation (DFG) with grant SA 683/9-1 (FOR2625) to P.S. and DA 1785/2-1 and DA 1785/2-2 to M.D (FOR2625).

References

Ballabio, A. and Bonifacino, J. S. (2020). Lysosomes as dynamic regulators of cell and organismal homeostasis. *Nature reviews. Molecular cell biology* **21**, 101-118.

Bonifacino, J. S. and Neefjes, J. (2017). Moving and positioning the endolysosomal system. *Current opinion in cell biology* **47**, 1-8.

Bonifacino, J. S. and Traub, L. M. (2003). Signals for sorting of transmembrane proteins to endosomes and lysosomes. *Annual review of biochemistry* **72**, 395-447.

Chapman, R. E. and Munro, S. (1994). Retrieval of TGN proteins from the cell surface requires endosomal acidification. *The EMBO journal* **13**, 2305-12.

Charollais, J. and Van Der Goot, F. G. (2009). Palmitoylation of membrane proteins (Review). *Molecular membrane biology* **26**, 55-66.

Diez-Ardanuy, C., Greaves, J., Munro, K. R., Tomkinson, N. C. and Chamberlain, L. H. (2017). A cluster of palmitoylated cysteines are essential for aggregation of cysteine-string protein mutants that cause neuronal ceroid lipofuscinosis. *Scientific reports* **7**, 10.

Dowal, L., Yang, W., Freeman, M. R., Steen, H. and Flaumenhaft, R. (2011). Proteomic analysis of palmitoylated platelet proteins. *Blood* **118**, e62-73.

Ernst, A. M., Syed, S. A., Zaki, O., Bottanelli, F., Zheng, H., Hacke, M., Xi, Z., Rivera-Molina, F., Graham, M., Rebane, A. A. et al. (2018). S-Palmitoylation Sorts Membrane Cargo for Anterograde Transport in the Golgi. *Developmental cell* **47**, 479-493 e7.

Ernst, A. M., Toomre, D. and Bogan, J. S. (2019). Acylation - A New Means to Control Traffic Through the Golgi. *Frontiers in cell and developmental biology* **7**, 109.

Flannery, A. R., Czibener, C. and Andrews, N. W. (2010). Palmitoylation-dependent association with CD63 targets the Ca2+ sensor synaptotagmin VII to lysosomes. *The Journal of cell biology* **191**, 599-613.

Forrester, M. T., Hess, D. T., Thompson, J. W., Hultman, R., Moseley, M. A., Stamler, J. S. and Casey, P. J. (2011). Site-specific analysis of protein S-acylation by resin-assisted capture. *Journal of lipid research* **52**, 393-8.

Gonzalez, A. C., Schweizer, M., Jagdmann, S., Bernreuther, C., Reinheckel, T., Saftig, P. and Damme, M. (2018). Unconventional Trafficking of Mammalian Phospholipase D3 to Lysosomes. *Cell reports* **22**, 1040-1053.

Guardia, C. M., Farias, G. G., Jia, R., Pu, J. and Bonifacino, J. S. (2016). BORC Functions Upstream of Kinesins 1 and 3 to Coordinate Regional Movement of Lysosomes along Different Microtubule Tracks. *Cell reports* **17**, 1950-1961.

Hashimoto, Y., Shirane, M. and Nakayama, K. I. (2018). TMEM55B contributes to lysosomal homeostasis and amino acid-induced mTORC1 activation. *Genes to cells : devoted to molecular & cellular mechanisms* **23**, 418-434.

Ivaldi, C., Martin, B. R., Kieffer-Jaquinod, S., Chapel, A., Levade, T., Garin, J. and Journet, A. (2012). Proteomic analysis of S-acylated proteins in human B cells reveals palmitoylation of the immune regulators CD20 and CD23. *PloS one* **7**, e37187.

Kent, H. M., Evans, P. R., Schafer, I. B., Gray, S. R., Sanderson, C. M., Luzio, J. P., Peden, A. A. and Owen, D. J. (2012). Structural basis of the intracellular sorting of the SNARE VAMP7 by the AP3 adaptor complex. *Developmental cell* **22**, 979-88.

Kissing, S., Hermsen, C., Repnik, U., Nesset, C. K., von Bargen, K., Griffiths, G., Ichihara, A., Lee, B. S., Schwake, M., De Brabander, J. et al. (2015). Vacuolar ATPase in phagosome-lysosome fusion. *The Journal of biological chemistry* **290**, 14166-80.

Levental, I., Lingwood, D., Grzybek, M., Coskun, U. and Simons, K. (2010). Palmitoylation regulates raft affinity for the majority of integral raft proteins. *Proceedings of the National Academy of Sciences of the United States of America* **107**, 22050-4.

Martin, B. R. (2013). Nonradioactive analysis of dynamic protein palmitoylation. *Current protocols in protein science* **73**, 14 15 1-14 15 9.

Martin, B. R., Wang, C., Adibekian, A., Tully, S. E. and Cravatt, B. F. (2011). Global profiling of dynamic protein palmitoylation. *Nature methods* **9**, 84-9.

Merrick, B. A., Dhungana, S., Williams, J. G., Aloor, J. J., Peddada, S., Tomer, K. B. and Fessler, M. B. (2011). Proteomic profiling of S-acylated macrophage proteins identifies a role for palmitoylation in mitochondrial targeting of phospholipid scramblase 3. *Molecular & cellular proteomics : MCP* **10**, M110 006007.

Nada, S., Hondo, A., Kasai, A., Koike, M., Saito, K., Uchiyama, Y. and Okada, M. (2009). The novel lipid raft adaptor p18 controls endosome dynamics by anchoring the MEK-ERK pathway to late endosomes. *The EMBO journal* **28**, 477-89.

Percher, A., Ramakrishnan, S., Thinon, E., Yuan, X., Yount, J. S. and Hang, H. C. (2016). Mass-tag labeling reveals site-specific and endogenous levels of protein S-fatty acylation. *Proceedings of the National Academy of Sciences of the United States of America* **113**, 4302-7.

Pu, J., Keren-Kaplan, T. and Bonifacino, J. S. (2017). A Ragulator-BORC interaction controls lysosome positioning in response to amino acid availability. *The Journal of cell biology* **216**, 4183-4197.

Pu, J., Schindler, C., Jia, R., Jarnik, M., Backlund, P. and Bonifacino, J. S. (2015). BORC, a multisubunit complex that regulates lysosome positioning. *Developmental cell* **33**, 176-88.

Reaves, B. and Banting, G. (1994). Vacuolar ATPase inactivation blocks recycling to the trans-Golgi network from the plasma membrane. *FEBS letters* **345**, 61-6.

Reaves, B. J., Banting, G. and Luzio, J. P. (1998). Lumenal and transmembrane domains play a role in sorting type I membrane proteins on endocytic pathways. *Molecular biology of the cell* **9**, 1107-22.

Ren, X., Farias, G. G., Canagarajah, B. J., Bonifacino, J. S. and Hurley, J. H. (2013). Structural basis for recruitment and activation of the AP-1 clathrin adaptor complex by Arf1. *Cell* **152**, 755-67.

Rous, B. A., Reaves, B. J., Ihrke, G., Briggs, J. A., Gray, S. R., Stephens, D. J., Banting, G. and Luzio, J. P. (2002). Role of adaptor complex AP-3 in targeting wild-type and mutated CD63 to lysosomes. *Molecular biology of the cell* **13**, 1071-82.

Saftig, P. and Puertollano, R. (2020). How Lysosomes Sense, Integrate, and Cope with Stress. *Trends in biochemical sciences*.

Takemasu, S., Nigorikawa, K., Yamada, M., Tsurumi, G., Kofuji, S., Takasuga, S. and Hazeki, K. (2019). Phosphorylation of TMEM55B by Erk/MAPK regulates lysosomal positioning. *Journal of biochemistry* **166**, 175-185.

Tanimura, N., Saitoh, S., Kawano, S., Kosugi, A. and Miyake, K. (2006). Palmitoylation of LAT contributes to its subcellular localization and stability. *Biochemical and biophysical research communications* **341**, 1177-83.

Ungewickell, A., Hugge, C., Kisseleva, M., Chang, S. C., Zou, J., Feng, Y., Galyov, E. E., Wilson, M. and Majerus, P. W. (2005). The identification and characterization of two phosphatidylinositol-4,5-bisphosphate 4-phosphatases. *Proceedings of the National Academy of Sciences of the United States of America* **102**, 18854-9.

Vergarajauregui, S. and Puertollano, R. (2006). Two di-leucine motifs regulate trafficking of mucolipin-1 to lysosomes. *Traffic* **7**, 337-53.

Webb, Y., Hermida-Matsumoto, L. and Resh, M. D. (2000). Inhibition of protein palmitoylation, raft localization, and T cell signaling by 2-bromopalmitate and polyunsaturated fatty acids. *The Journal of biological chemistry* **275**, 261-70.

Willett, R., Martina, J. A., Zewe, J. P., Wills, R., Hammond, G. R. V. and Puertollano, R. (2017). TFEB regulates lysosomal positioning by modulating TMEM55B expression and JIP4 recruitment to lysosomes. *Nature communications* **8**, 1580.

Zhang, W., Trible, R. P. and Samelson, L. E. (1998). LAT palmitoylation: its essential role in membrane microdomain targeting and tyrosine phosphorylation during T cell activation. *Immunity* **9**, 239-46.

Figures

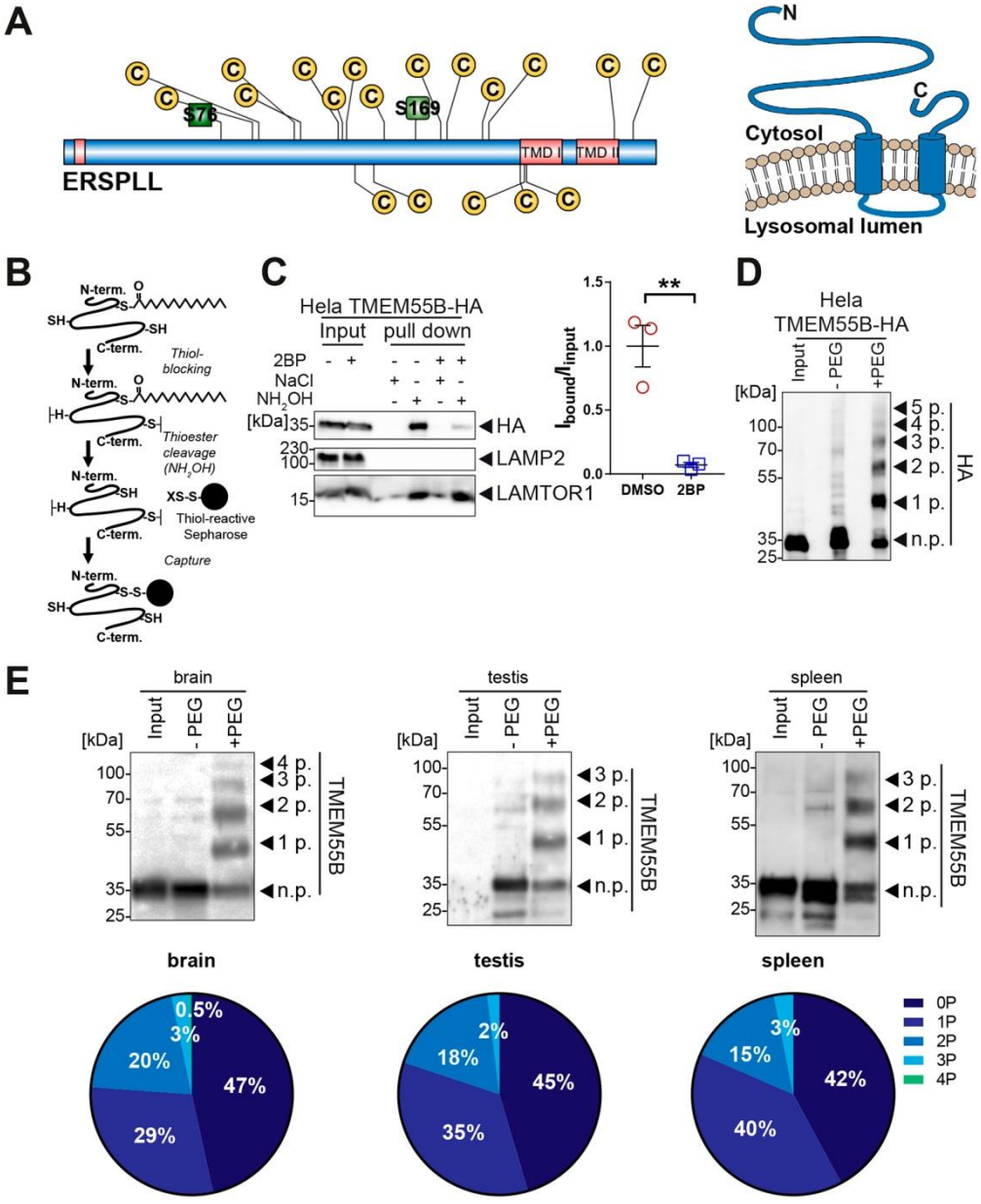

Figure 1. ***TMEM55B is a bona fide S-palmitoylated protein and palmitoylated on several cysteine-residues.*** **(A)** Domain structure of murine TMEM55B. Cysteine-residues, phosphorylated serine residues, the dileucine-based sorting motif, and the two transmembrane domains (TMDs) are indicated. A topology model of TMEM55B with both its N- and C-terminus in the cytosol is depicted on the right. **(B)** Schematic drawing of the experimental acyl-RAC approach for capturing S-palmitoylated protein. **(C)** Immunoblot of

the different fractions of TMEM55B-HA transfected Hela cell lysates analyzed by the acyl-RAC assay with antibodies against HA, LAMP2, and LAMTOR1. 2-BP (100 µM) was included as an inhibitor of S-palmitoylation in one sample. The addition of hydroxylamine (NH_2OH) leads to thioester cleavage. NaCl was used as a negative control, in which thioesters are not cleaved. “Input” corresponds to the cell lysates, “pull-down” to thiol-reactive sepharose chromatography enriched samples. Quantification of three experiments is shown as the ratio of the immunoblot signals of S-palmitoylated TMEM55B-HA relative to the (N = 3; * = $p \leq 0.05$). **(D)** Immunoblot with antibodies against HA of the different fractions of TMEM55B-HA transfected Hela cell lysates analyzed by the acyl-PEG assay. The “input fraction” corresponds to the lysates. The number of differentially S-palmitoylated TMEM55B-HA forms (p) is indicated with arrowheads. Cells were lysed, treated with the reducing agent TCEP and thiol groups blocked with NEM. After cleavage, proteins were treated with PEG (+PEG) or as a negative control without PEG (-PEG). **(E)** Immunoblot with an antibody against TMEM55B of different tissue lysates (brain, testis, spleen) analyzed by the acyl-PEG assay performed as described above. Quantification of immunoblot signal of the differentially S-palmitoylated (p) forms per tissue is depicted and represented in the percentage of the total TMEM55B signal (N = 3); n.p. = non-palmitoylated.

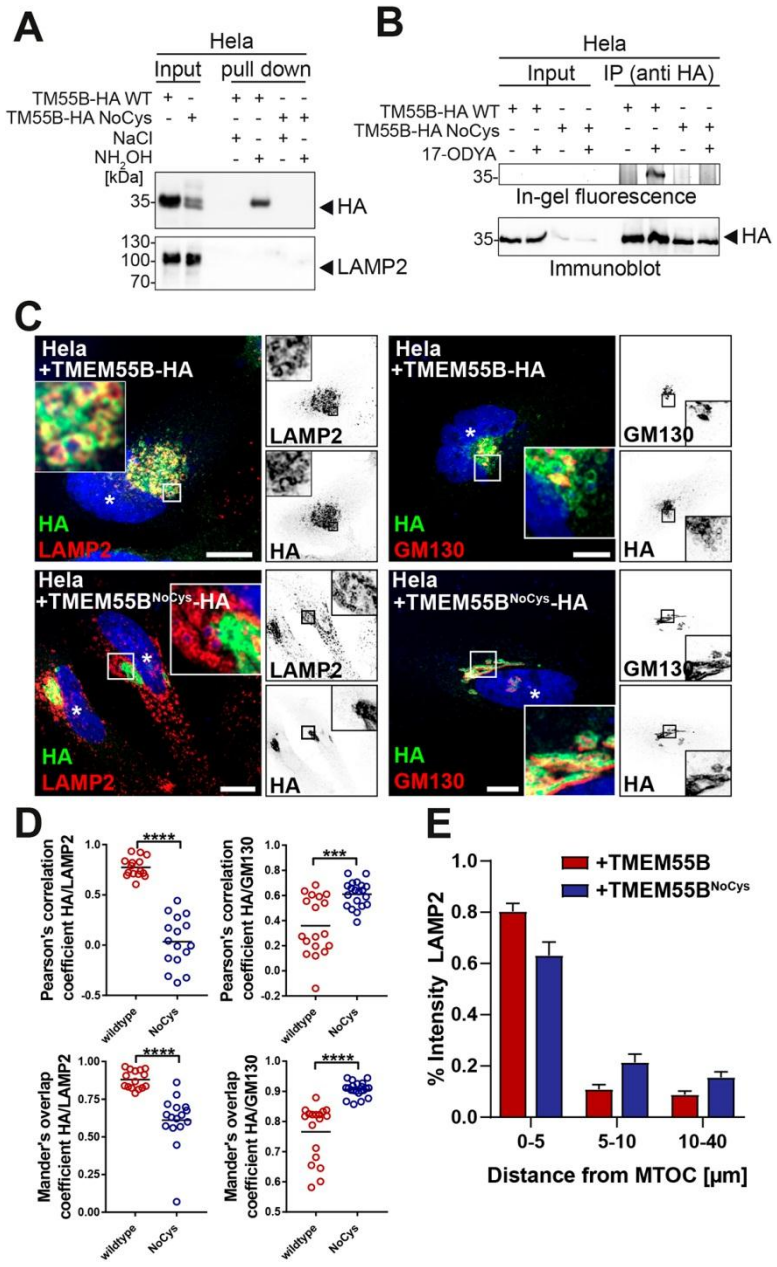

Figure 2. ***Mutation of all cysteines in TMEM55B abrogates S-palmitoylation and leads to localization in the Golgi-apparatus.*** **(A)** Immunoblot of the different fractions of TMEM55B-HA or TMEM55B^{NoCys}-HA transfected Hela cell lysates analyzed by the acyl-RAC assay with antibodies against HA and LAMP2. The addition of hydroxylamine (NH_2OH) leads to thioester cleavage. NaCl was used as a negative control, in which thioesters are not cleaved **(B)** In-gel fluorescence (upper panel) and immunoblot analysis (lower panel) of lysates (left) and HA-immunoprecipitates (right) from cells transfected with TMEM55B-HA or

TMEM55B^{NoCys}-HA, metabolically labeled (and non-labeled) with 17-ODYA, click-chemistry-based attachment of fluorescent dye and SDS-PAGE / SDS-PAGE and immunoblot “Input” corresponds to the cell lysates, “IP” corresponds to the HA-immunoprecipitated fractions. **(C)** Co-immunofluorescence staining of cells transfected with TMEM55B-HA or TMEM55B^{NoCys}-HA with antibodies against HA (green) and LAMP2 (left panels) or GM130 (right panels) (red). Nuclei are stained with DAPI (blue). Transfected cells are labeled with asterisks. **(D)** The Pearson correlation coefficient (PCC) and the Manders overlap coefficient between TMEM55B-HA and LAMP2 / TMEM55B-HA and GM130 for TMEM55B-HA and TMEM55B^{NoCys}-HA are depicted. **(E)** The LAMP2-signal intensity in relation to the distance to the microtubule organizing center (MTOC) in cells transfected with wild-type TMEM55B-HA or TMEM55B^{NoCys}-HA, respectively, is depicted. **** = $p < 0.0001$. Scale: 10 µm.

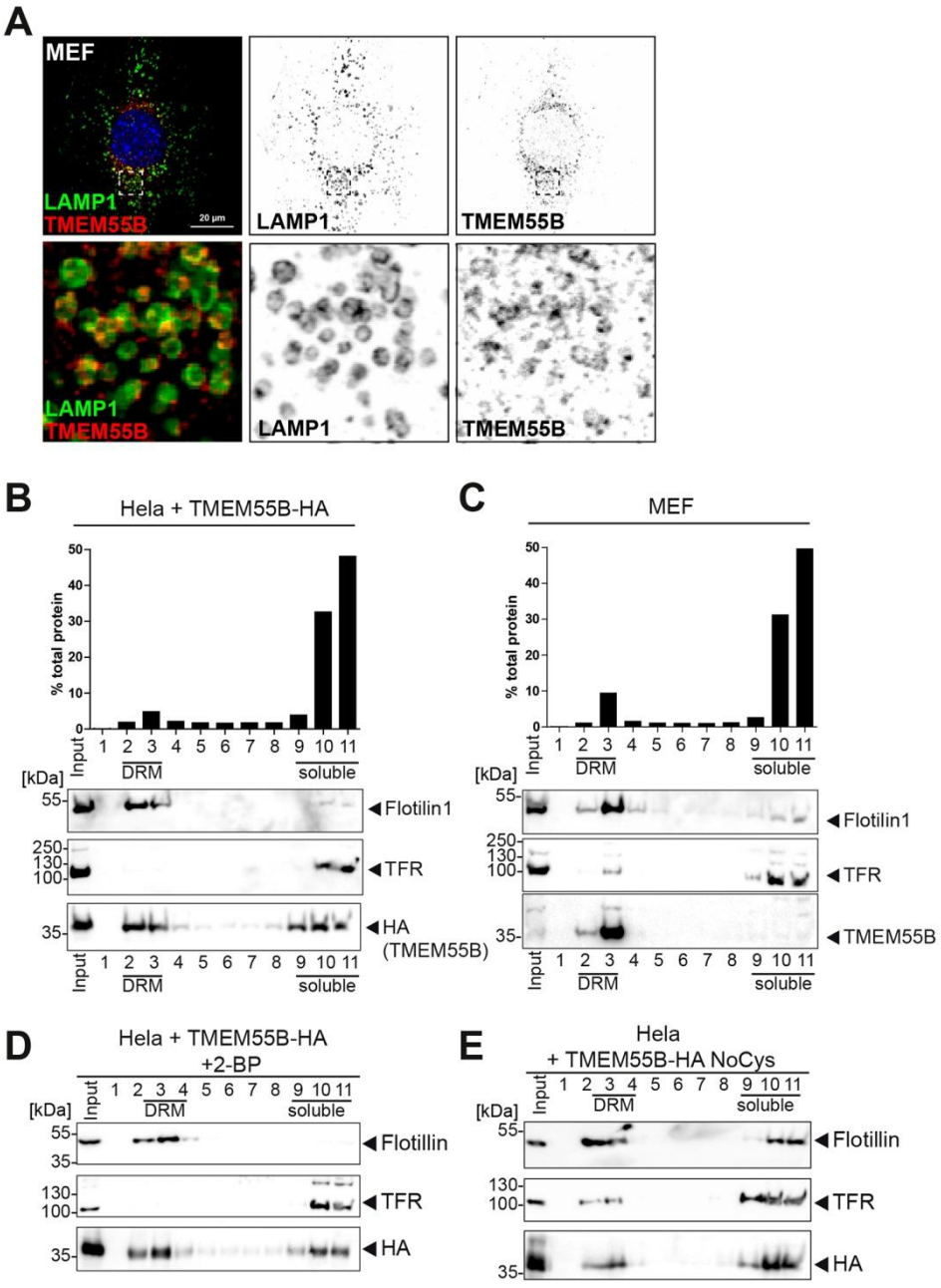

Figure 3. ***TMEM55B partitions into detergent-resistant membranes (DRM), and S-palmitoylation is dispensable for DRM-localisation.*** **(A)** Co-immunofluorescence staining of endogenous TMEM55B (red) and LAMP1 (green) in MEFs. Nuclei are stained with DAPI (blue) Scale: 20 µm. **(B)** DRMs of Hela cells transfected with TMEM55B-HA were separated from soluble proteins by discontinuous sucrose gradient ultracentrifugation (gradient: 42,5%, 35%, and 5% (w/v) sucrose). The collected fractions were analyzed by immunoblot with antibodies against the DRM-marker Flotilin1, the non-DRM-localised TFR, and HA. The

distribution of the total protein in each fraction is depicted. **(C)** DRMs from MEFs were separated from non-DRM fractions by discontinuous sucrose gradient ultracentrifugation. After centrifugation, the individual sucrose-gradient fractions were analyzed by immunoblot with antibodies against the DRM-marker Flotilin1, the non-DRM-localised transferrin receptor (TFR), and TMEM55B. The distribution of the total protein in each fraction is depicted. **(D)** DRMs of Hela cells transfected with TMEM55B-HA and treated with 2-BP were separated from non-DRM fractions by sucrose gradient centrifugation. The fractions were analyzed by immunoblot with antibodies against the DRM-marker Flotilin1, the non-DRM-localised TFR, and HA. The distribution of the total protein in each fraction is depicted. **(E)** DRMs of Hela cells transfected with TMEM55B-HA^{NoCys} were separated from non-DRM fractions by sucrose gradient centrifugation. The fractions were analyzed by immunoblot with antibodies against the DRM-marker Flotilin1, the non-DRM-localised TFR, and HA. The distribution of the total protein in each fraction is depicted.

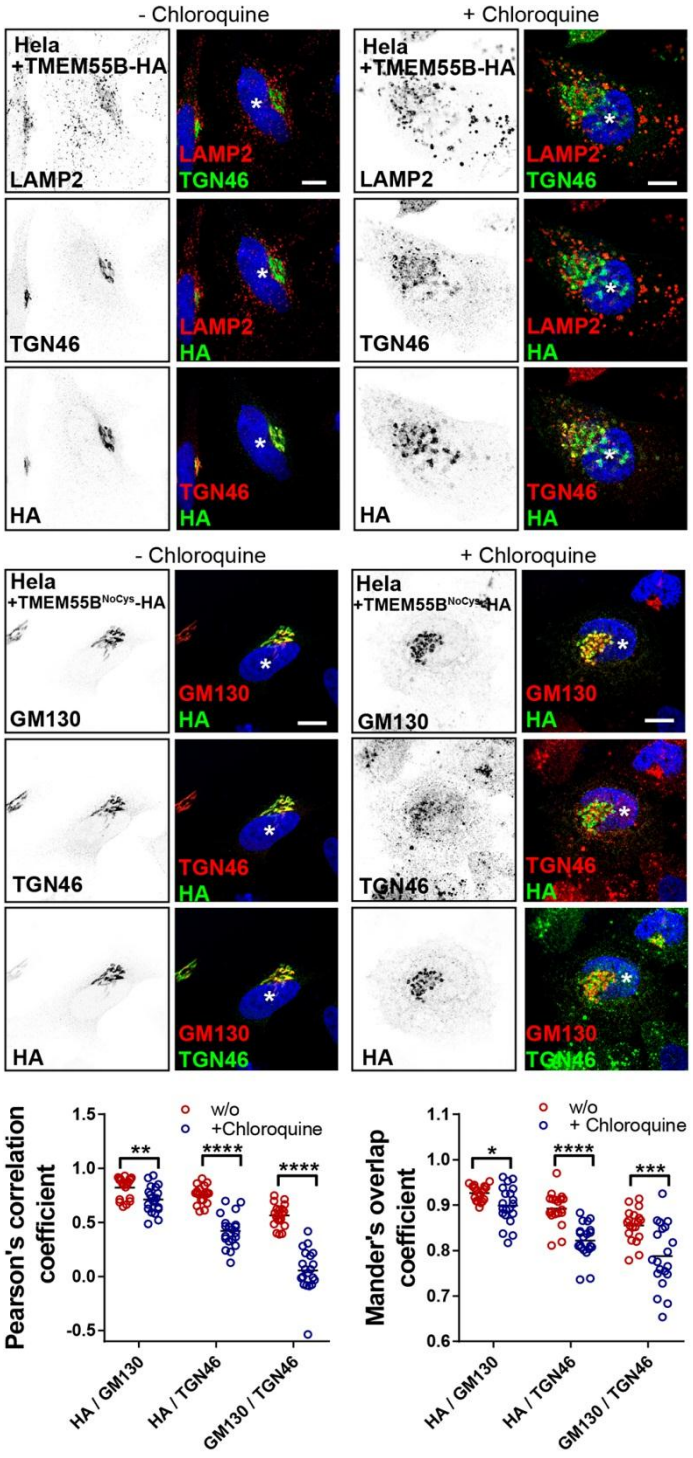

Figure 4. ***Golgi mislocalization of TMEM55B^{NoCys} is not due to retrograde transport from endosomes to the Golgi.*** Immunofluorescence staining of untreated Hela cells (**left panels**) transfected with TMEM55B-HA (upper panels) or TMEM55B^{NoCys}-HA (lower panels) for LAMP2, HA, and TGN46 or Hela cells treated with chloroquine (2 hours, 200 µM) (**right**

panels). Different combinations of merged images are shown. Nuclei are stained with DAPI (blue). Transfected cells are labeled with asterisks. Scale: 10 µm. The Pearson correlation coefficient and the Manders overlap coefficient between different antibody combinations are depicted. * = p <0.05; ** = p <0.01; *** = p <0.001; **** = p <0.0001.

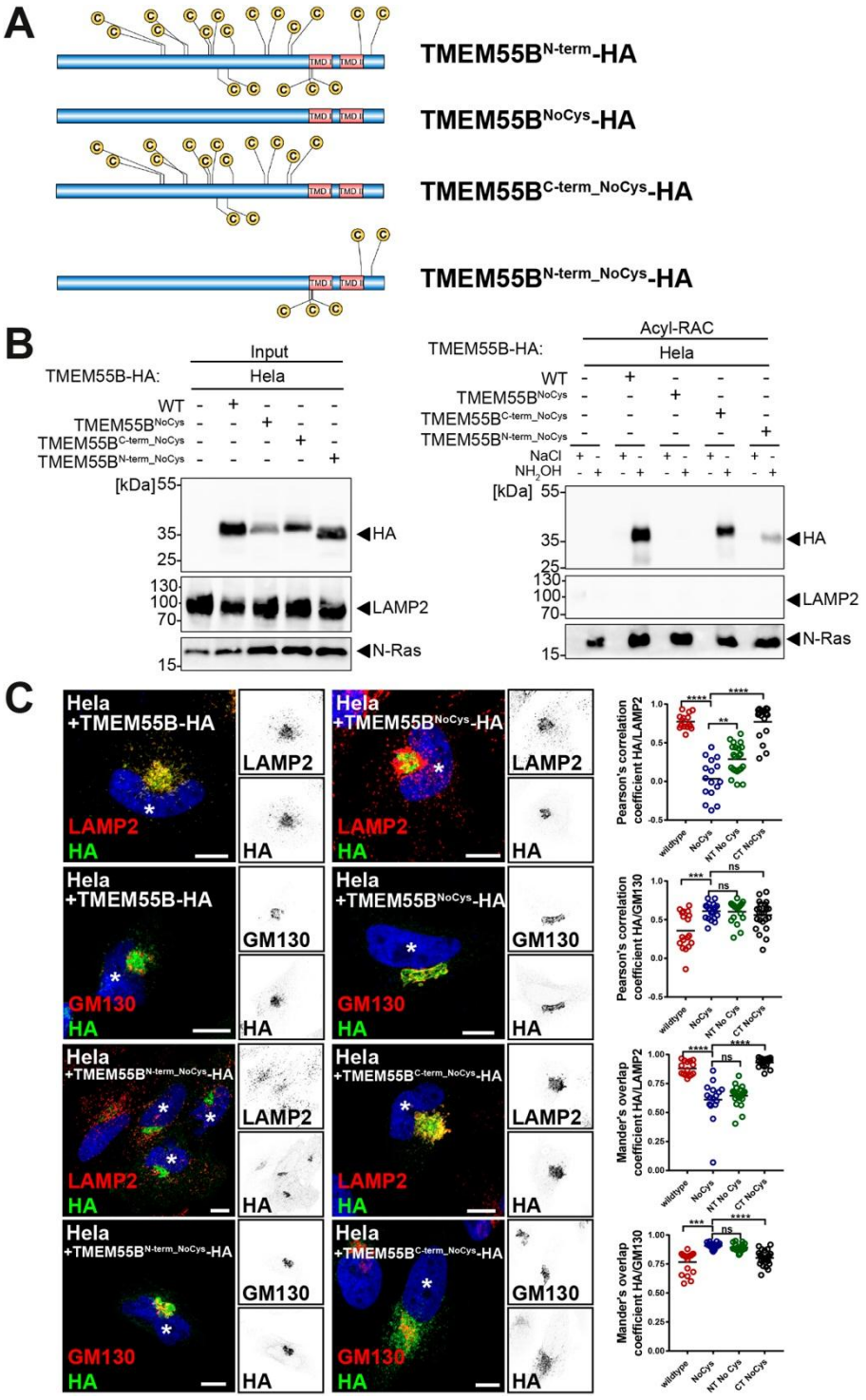

Figure 5. ***The N-terminal cytosolic domain and the transmembrane-containing C-terminus contain S-palmitoylated cysteines, and mutation of all cysteines in the N-terminus of TMEM55B leads to Golgi missorting.*** **(A)** Overview of the TMEM55B constructs with cysteine-to-serine exchange used for the following experiments. **(B)** Left

panel: Immunoblot analysis of lysates from Hela cells transfected with full-length TMEM55B-HA, the TMEM55B^{NoCys} variant, and constructs lacking cysteines in the N-terminus (TMEM55B$^{N\text{-}term_NoCys}$-HA) or the C-terminus (TMEM55B$^{C\text{-}term_NoCys}$-HA) (see **(A)**) with an antibody against HA. N-Ras and LAMP2 are shown as a loading control. Right panel: Immunoblot of the fractions from the acyl-RAC assay of lysates from cells transfected with full-length TMEM55B and the cysteine-mutants with an antibody against HA. N-Ras is shown as a loading control for S-palmitoylated proteins. LAMP2 is shown as a loading control for non-S-palmitoylated proteins. The addition of hydroxylamine (NH_2OH) or NaCl (used as a negative control) to the acyl-RAC assay is indicated. **(C)** Co-Immunofluorescence staining of Hela cells transfected with full-length TMEM55B-HA, the TMEM55B^{NoCys}, TMEM55B$^{N\text{-}term_NoCys}$-HA, or TMEM55B$^{C\text{-}term_NoCys}$-HA variants for LAMP2 (red) and HA (green) or GM130 (red) and HA (green), respectively. Nuclei are stained with DAPI (blue). Scale: 10 µm. The Pearson correlation coefficient and the Manders overlap coefficient between TMEM55B-HA constructs and LAMP2 / TMEM55B-HA and GM130 are depicted. ns = not significant; ** = $p < 0.01$; *** = $p < 0.001$; **** = $p < 0.0001$.

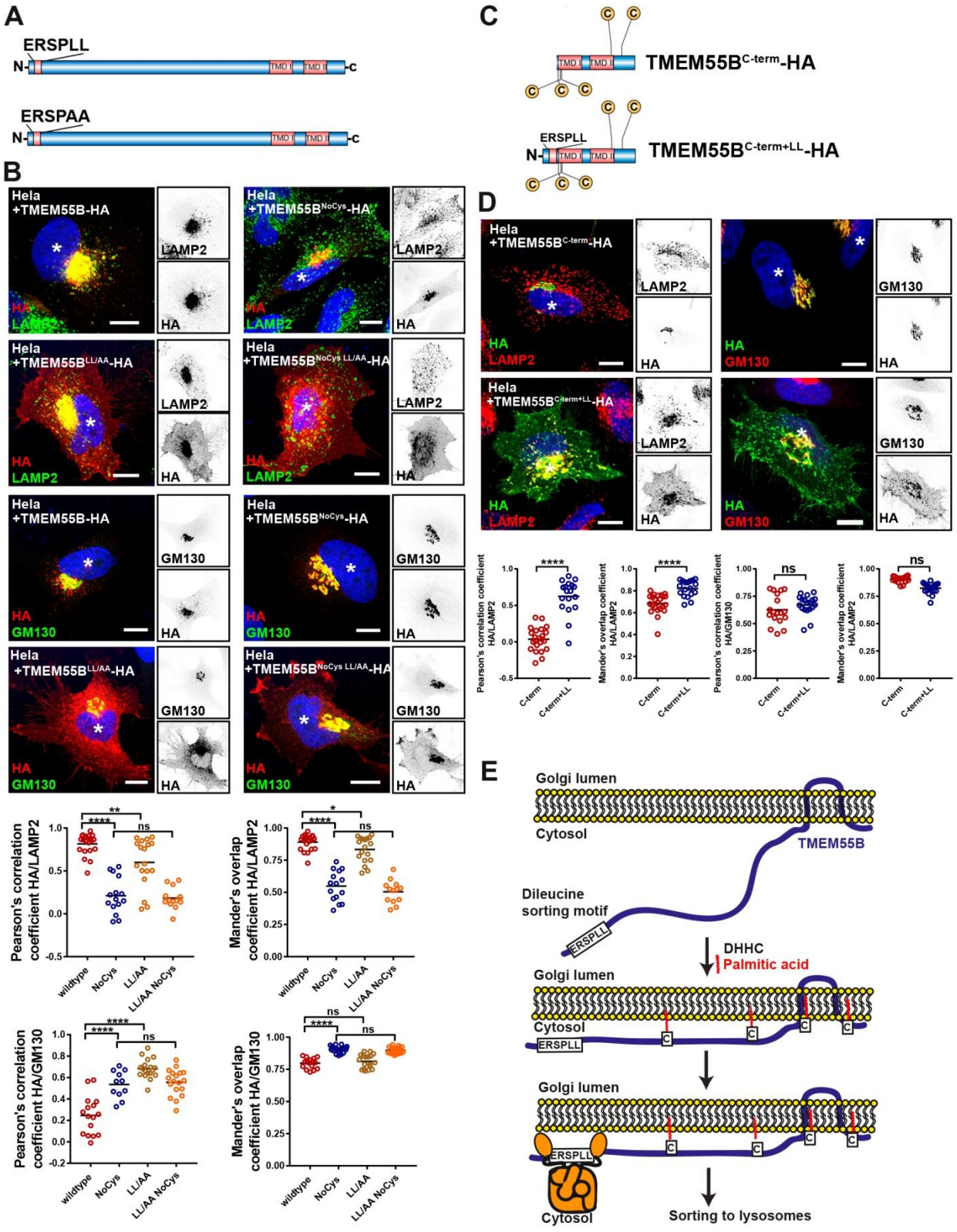

Figure 6. ***S-palmitoylation facilitates post-Golgi sorting of TMEM55B.*** **(A)** Schematic representation of TMEM55B with its N-terminal dileucine motif and the mutant with both critical leucine-residues (TMEM55B$^{LL/AA}$) mutated to alanine. **(B)** Co-immunofluorescence staining of Hela cells transfected with TMEM55B-HA, TMEM55B$^{LL/AA}$-HA, TMEM55B^{NoCys}-HA, or TMEM55B$^{LL/AA_NoCys}$-HA with antibodies against HA (red), LAMP2 (left panel, green), and GOLGA2 (right panel, green). Nuclei are stained with DAPI (blue). Scale: 10 µm. The Pearson correlation coefficient (PCC) and the Manders overlap coefficient between TMEM55B-HA constructs and LAMP2 / TMEM55B-HA and GM130 are depicted **(C)** Schematic drawing of the TMEM55B$^{C\text{-}term}$-HA, TMEM55B$^{C\text{-}term+LL}$-HA constructs. **(D)** Co-immunofluorescence staining of Hela cells transfected with TMEM55BC-term-HA, TMEM55BC-term+LL-HA with antibodies against HA, LAMP2, and GM130. Different combinations of merged images are shown. Nuclei are stained with DAPI (blue). Scale: 10µm. **(E)** Schematic drawing of the proposed mechanism of how S-palmitoylation facilitates export and post-Golgi sorting of TMEM55B: TMEM55B is modified with palmitate in the Golgi apparatus, S-palmitoylation brings the dileucine-based sorting motif in closer proximity to the membrane. Adaptor proteins can bind and mediate concentration and packing into clathrin-coated vesicles for sorting to lysosomes.

Supplemental Figure 1

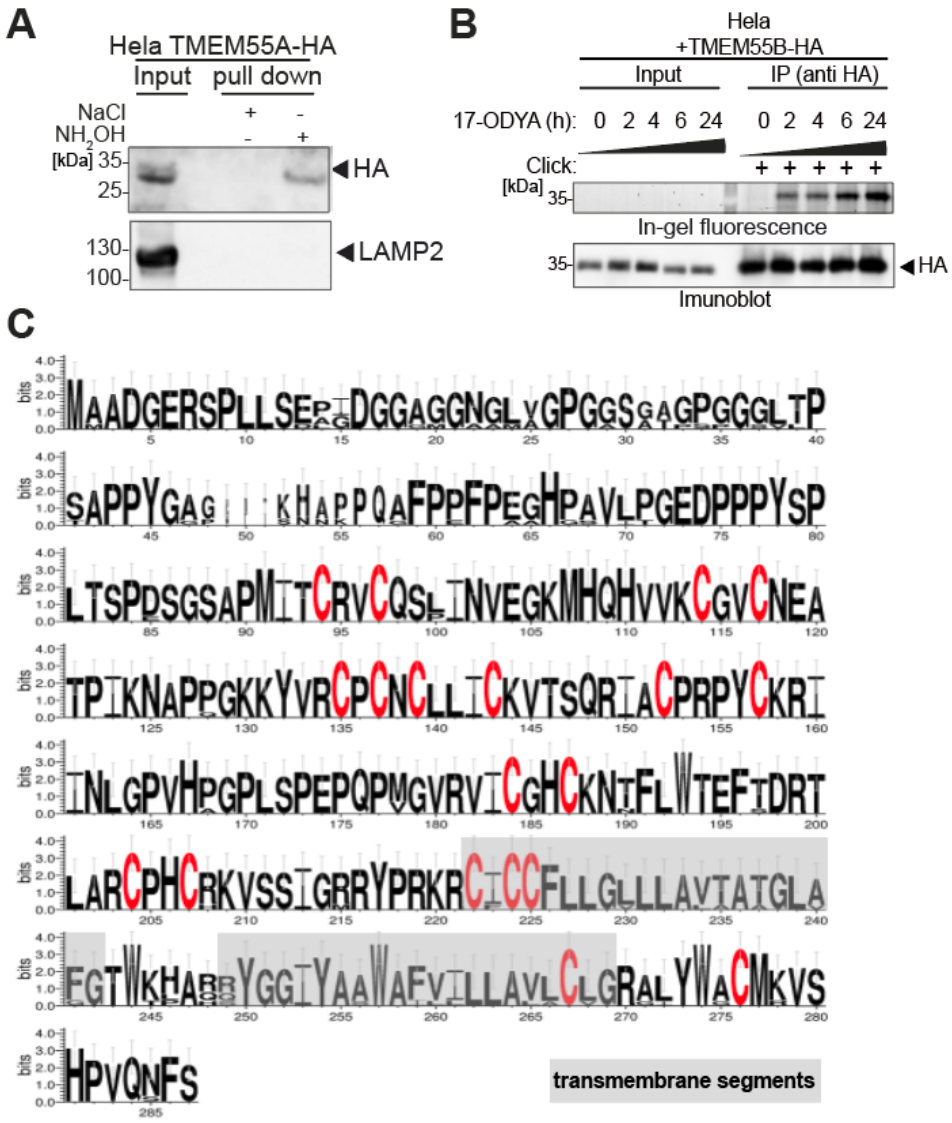

Fig. S1. ***TMEM55A is S-palmitoylated, and cysteines in TMEM55B are highly conserved.*** **(A)** Immunoblot of the different fractions of TMEM55A-HA transfected Hela cell lysates analyzed by the acyl-RAC assay with antibodies against HA and LAMP2. The "input" fraction corresponds to the lysate. The "pull-down fractions" correspond to the thiol-reactive chromatography fractions. Neutral hydroxylamine (NH_2OH) cleaves thioesters, NaCl was used as a negative control. **(B)** Detection of S-palmitoylation of TMEM55B by click chemistry. Hela cells were metabolically pulse-labeled with 17-ODYA (50 µm) for increasing pulse times (0 – 24 hours), lysed, and protein lysates were separated by SDS-PAGE. In-gel fluorescence (upper panel) and immunoblot with an antibody against HA of the input lysate fractions of Hela cells transfected with TMEM55B-HA (left) and immunoprecipitates with the antibody against HA are depicted (right lanes). **(C)** Weblogo representation of the amino acid sequence of TMEM55B from *Homo sapiens, Mus musculus, Rattus norvegicus, Pan troglodytes, Macaca mulatta, Bos taurus,* and *Xenopus laevi.* Cysteine residues are highlighted in red. Generated with "WebLogo 3", (Crooks GE et al. Genome Research, 2004). The transmembrane regions are shaded in grey.

Supplemental Figure 2

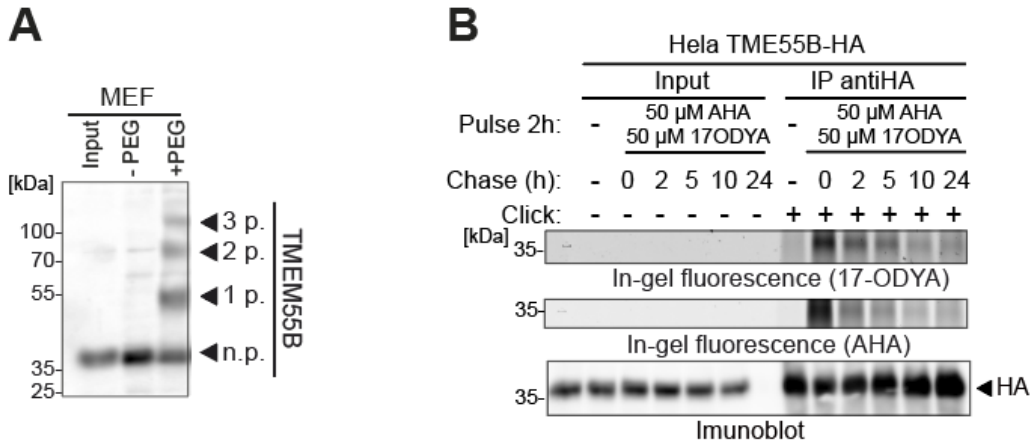

Fig. S2. ***Endogenous TMEM55B in MEFs is multiple times S-palmitoylated,.*** **(A)** Immunoblot of MEF cells analyzed by the acyl-PEG assay with an antibody against TMEM55B. The attached PEG leads to a distinctive shift of the target protein in the apparent molecular weight after SDS-PAGE. **(B)** Dynamic analysis of S-palmitoylation by pulse-chase and click chemistry of palmitate and the protein backbone by AHA. Hela cells were metabolically pulse-labeled with 17-ODYA and the methionine analog AHA for 2 hours and chased for increasing time points (0 – 24 hours). Cell lysates were sequentially labeled with fluorophores by click chemistry (AF647-Azide for AHA; with AF488-Alkyne for 17-ODYA). In-gel fluorescence of the 647 channel (AHA) and the 488 channel (17-ODYA) and immunoblot with an antibody against HA of the input lysate fractions of Hela cells transfected with TMEM55B-HA (left) and immunoprecipitates with the antibody against HA are depicted (right lanes).

Supplemental Figure 3

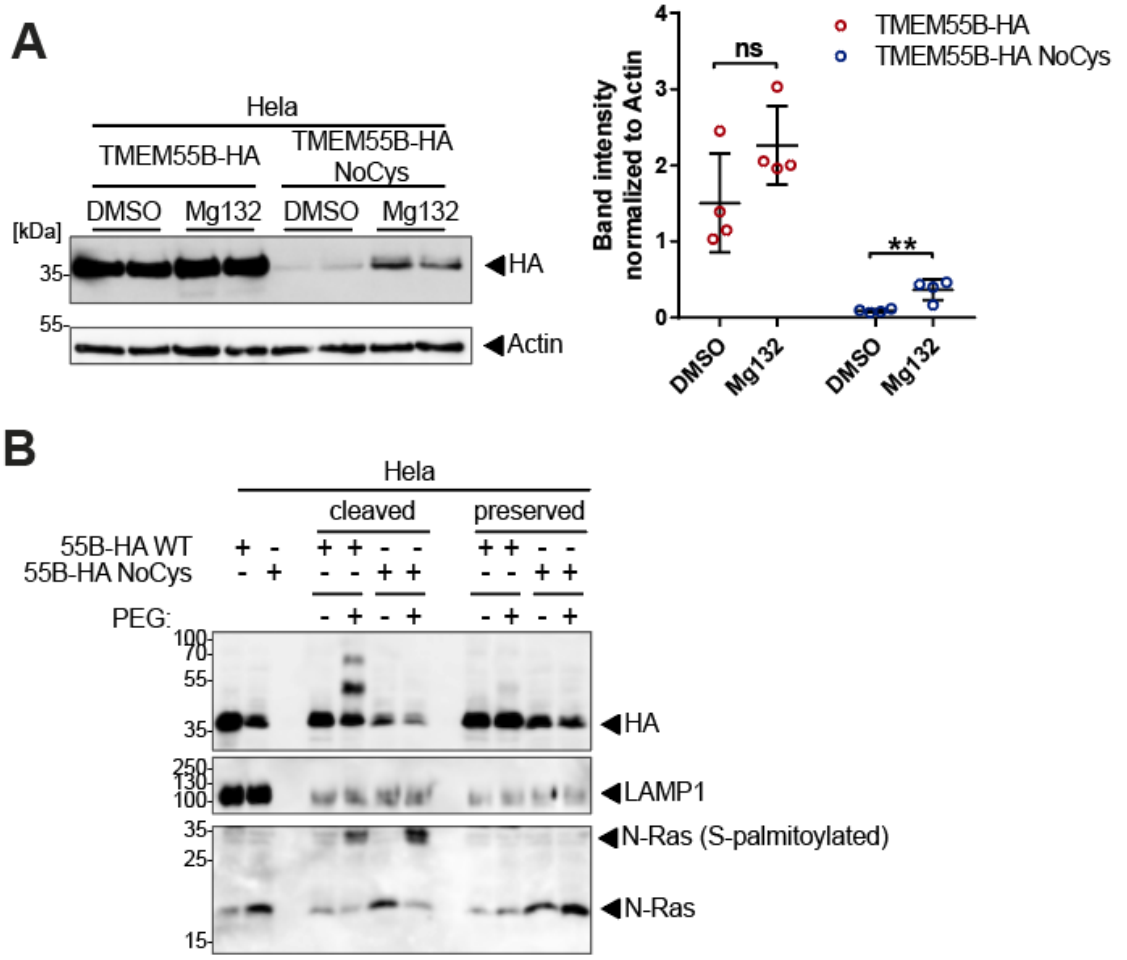

Fig. S3. ***TMEM55B^{NoCys}-HA is stabilized by the inhibition of the proteasome.*** **(A)** Immunoblot of lysates from Hela cells transfected with TMEM55B-HA or TMEM55B^{NoCys}-HA, treated for 16 hours with the proteasome inhibitor MG132 (3 μM) or DMSO with an antibody against HA. Actin is depicted as a loading control. The quantification of 4 independent transfections is depicted. **(B)** Immunoblot with antibodies against HA N-Ras and LAMP1 of the different fractions of TMEM55B-HA or TMEM55B^{NoCys}-HA-transfected Hela cell lysates analyzed by the acyl-PEG assay. The "preserved" fractions correspond to lysates where NH_2OH was omitted. The "cleaved" fractions correspond to fractions where thioesters were cleaved with NH_2OH. Cells were lysed, treated with the reducing agent TCEP and thiol groups blocked with or without NEM. After precipitation, proteins were treated with PEG (+PEG) or as a negative control without PEG (-PEG)

Supplemental Figure 4

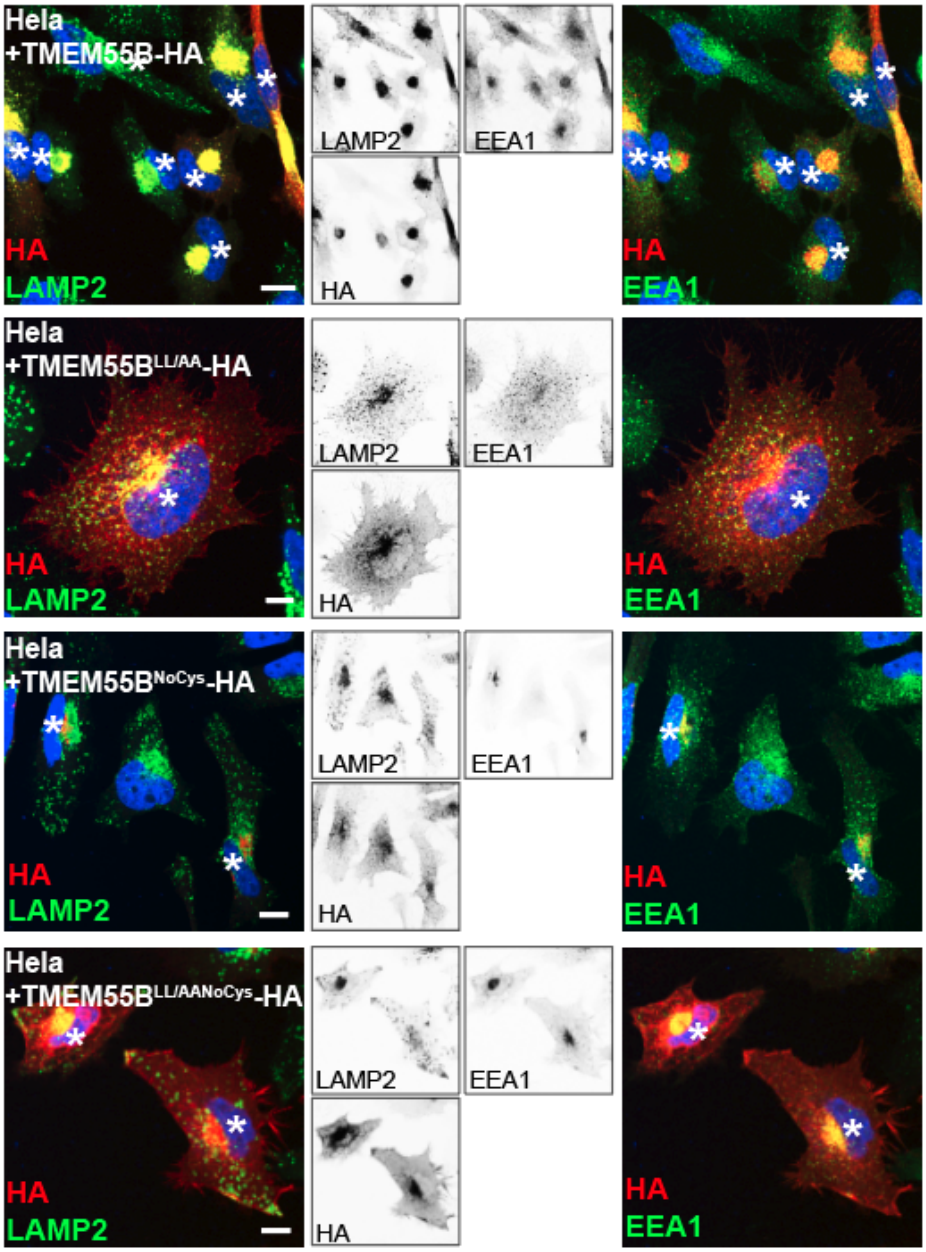

Fig. S4. ***Plasma-membrane-localized TMEM55B constructs show little co-localization with the lysosomal marker LAMP2 and the early endosomal marker EEA1.*** Co-Immunofluorescence staining of Hela cells transfected with full-length TMEM55B-HA, the TMEM55B^{NoCys}, TMEM55B^{LL_AA}-HA, or TMEM55B^{LL_AA_NoCys}-HA variants for LAMP2 (green) and HA (red) (left panel) or EEA1 (green) and HA (red) (right panel), respectively. Nuclei are stained with DAPI (blue). Scale: 10 µm.